Iranian Journal of Materials Forming 14 (1) (2027) 4-22

IJMF

Online ISSN: 2383-0042

Iranian Journal of Materials Forming

Journal Homepage: http://ijmf.shirazu.ac.ir

Research Article

Performance of Carbon Black Reinforced Aluminum Composites Fabricated by Accumulative Roll Bonding (ARB) under Preheated Conditions

Seyyed Ehsan Eftekhari Shahri [1,2 *], Seyed Ehsan Fatemi[1], Amin Saghafi[1], Yadollah Yaghoubinezhad[3] and Ayrat M. Dimiev[4]

[1] Department of Mechanical Engineering, Birjand University of Technology, Birjand, Iran
[2] Centre for International Scientific Studies & Collaborations (CISSC), Ministry of Science, Research and Technology of Iran, Tehran, Iran
[3] Department of Materials Engineering, Birjand University of Technology, Birjand, Iran
[4] Laboratory for Advanced Carbon Nanomaterials, Chemical Institute, Kazan Federal University, Kremlevskaya St. 18, Kazan 420008, Russian Federation

ARTICLE INFO

Article history:

Received: 11 March 2026
Reviewed: 30 May 2026
Revised: 17 June 2026
Accepted: 1 July 2026

Keywords:

Carbon black
Aluminum matrix composites
Accumulative roll bonding
Mechanical properties
Electrical resistance

Please cite this article as:

Eftekhari Shahri, S. E., Fatemi, S, E., Saghafi, A., Yaghoubinezhad, Y., & Dimiev, A. M. (2027). Performance of carbon black reinforced aluminum composites fabricated by accumulative roll bonding (ARB) under preheated conditions. *Iranian Journal of Materials Forming*, *14*(1), 4-22. https://doi.org/10.22099/IJMF.2026.55837.1377

ABSTRACT

In this study, carbon black (CB) was evaluated as a low-cost and economically efficient reinforcement for aluminum matrix composites fabricated by accumulative roll bonding (ARB) under preheated conditions at 380 °C. The mechanical behavior, microhardness, and electrical resistance of CB/Al sheets were systematically compared with unprocessed aluminum, cold and preheated-ARB aluminum, and graphene oxide reinforced composites (GO/Al). Cold ARB increased the ultimate tensile strength (UTS) of aluminum from 136.9 MPa to 259.4 MPa after five passes, corresponding to an 89.5% improvement, while elongation decreased from 26.9% to 11.5%. Preheating enabled stable processing up to seven passes without edge cracking, although the UTS of unreinforced aluminum decreased to 189.9 MPa in the first pass due to thermal softening. Incorporation of CB in the first preheated ARB pass enhanced the UTS to 198.8 MPa, which is 4.7% higher than that of unreinforced preheated ARB aluminum and 45.2% higher than that of the initial aluminum, confirming the effectiveness of particulate strengthening. However, increasing cumulative strain to higher passes led to gradual degradation in strength and ductility, attributed to particle re-agglomeration. Notably, CB consistently improved microhardness, reaching a maximum increase of 12.3% at the third pass, which exceeded that of GO/Al composites. Electrical resistance was reduced by 20% in the first pass compared to unreinforced preheated ARB aluminum, while the difference between CB/Al and GO/Al remained below 10% across all processing passes. Overall, although GO/Al exhibits superior mechanical stability at higher strains, CB/Al provides comparable early-stage mechanical and electrical performance with higher local hardness and substantially lower material cost, highlighting carbon black as a promising reinforcement for cost-sensitive and scalable applications.

1. Introduction

Accumulative roll bonding (ARB) is one of the most widely employed severe plastic deformation (SPD)

* Corresponding author
E-mail address: e.eftekhari@birjandut.ac.ir (S. E. Eftekhari Shahri)
https://doi.org/10.22099/IJMF.2026.55837.1377

techniques for the fabrication of ultrafine-grained materials and metal matrix composites (MMCs), particularly in aluminum-based systems[1-4]. As a solid-state processing route, ARB enables the formation of strong metallurgical bonding, effective grain refinement, and the homogeneous distribution of reinforcing phases, while significantly mitigating typical casting-related defects such as phase segregation, porosity, and undesirable interfacial reactions [2, 3].

In the ARB process, metallic sheets are surface-prepared, stacked, and subjected to successive rolling with large thickness reductions. Each cycle consists of cutting, restacking, and rolling, which imposes extremely high cumulative strains and leads to the development of refined and continuous microstructures [3, 5]. A schematic illustration of the ARB procedure is presented in Fig. 1. Industrial scalability and the capability to tailor microstructural features are among the key advantages of this technique [6]. Moreover, ARB can function as a solid-state welding route for joining similar or dissimilar metals over a wide temperature range [7].

The incorporation of reinforcing phases such as ceramic particles, fibers, foils, and nanostructured reinforcements during ARB has been recognized as an effective strategy to simultaneously enhance the strength, hardness, and microstructural stability of composites [6, 8]. The uniformity of reinforcement distribution is a critical factor governing the reproducibility and long-term stability of mechanical properties. In this regard, ARB, particularly at higher pass numbers, exhibits a strong capability for homogenizing the reinforcing phase throughout the matrix [8].

In recent years, considerable attention has been devoted to the use of graphene derivatives as reinforcements in ARB-processed aluminum matrix composites. It has been reported that ARB can effectively exfoliate graphite and graphene and promote their dispersion within the metallic matrix, in some cases reducing the graphite thickness to a few graphene layers [9]. The homogeneous distribution of graphene and the formation of stable interfacial structures have resulted in substantial improvements in strength, hardness, and, in certain cases, electrical conductivity [10-13].

Despite these advantages, several challenges remain, including particle agglomeration, the formation of brittle interfacial phases, and strong sensitivity of the properties to graphene content and dispersion uniformity [14]. In addition, the high cost and processing complexity of graphene significantly limit its large-scale industrial application. From a practical perspective, the use of more cost-effective carbonaceous fillers, such as carbon black, may provide a viable alternative.

Although carbon black exhibits lower intrinsic electrical conductivity than graphene, its high specific surface area, chemical stability, wide industrial availability, and substantially lower processing cost offer considerable potential for tailoring the mechanical and electrical performance of metal matrix composites.

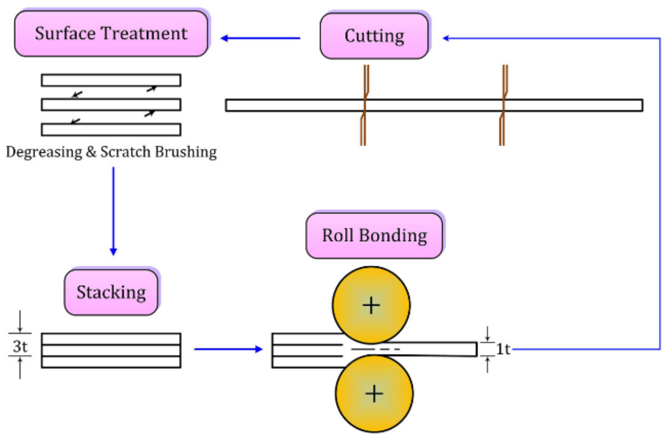

Fig. 1. Schematic illustration of the accumulative roll bonding process for three metallic layers [5].

The electrical response of carbon black-based systems is highly dependent on particle dispersion, morphology, and the formation of conductive networks, in which the percolation threshold plays a decisive role. Nevertheless, despite extensive studies on graphene-reinforced aluminum composites fabricated by ARB, a systematic investigation of aluminum–carbon black composites processed by this route has not yet been reported in the open literature. This gap provides an opportunity to assess the realistic potential of carbon black as an economical and scalable reinforcement in severe plastic deformation-based processing routes.

On the other hand, microstructural parameters such as the average crystallite size and dislocation density are strongly affected by the cumulative strain imposed during ARB and play a pivotal role in governing mechanical strength and structural stability [15]. The interaction between these microstructural features and the presence of carbonaceous reinforcements can simultaneously influence the mechanical and electrical behavior of the resulting composites.

It is important to acknowledge that severe plastic deformation (SPD) methods, including accumulative roll bonding (ARB), have not yet been widely adopted for large-scale industrial production of metal matrix composites. Nevertheless, compared to other SPD techniques such as high-pressure torsion (HPT) or equal-channel angular pressing (ECAP), ARB offers relatively greater potential for large-scale production. This is primarily because ARB utilizes conventional rolling mills, equipment that is already standard in the metal processing industries, whereas HPT and ECAP rely on specialized tooling and batch-type processing. However, several technical challenges remain, including maintaining a uniform dispersion of nanoscale reinforcements over large areas, controlling bonding quality across multiple cycles, and ensuring reproducible mechanical properties. Beyond processing limitations, the high cost of advanced reinforcements such as graphene oxide (GO) constitutes a major economic barrier to the industrialization of high-performance aluminum matrix composites, irrespective of the fabrication route.

In light of these considerations, the present study investigates a low-cost alternative, carbon black (CB), as a reinforcement. The aim is to determine whether measurable improvements in mechanical properties can be achieved without relying on expensive carbonaceous nanomaterials. The novelty of this work lies in: (i) the first systematic investigation of carbon black as a reinforcement in ARB-processed aluminum matrix composites, (ii) a direct comparison with graphene oxide under identical processing conditions, and (iii) a comprehensive evaluation of mechanical, hardness, and electrical properties supported by microstructural analysis. Accordingly, the primary objective of this work is to evaluate the reinforcing effect of carbon black on the microstructure, mechanical properties, and electrical performance of aluminum matrix composites fabricated by ARB.

Furthermore, this study seeks to elucidate the governing mechanisms associated with particle dispersion, interfacial bonding, and microstructural evolution during successive ARB passes. It should be emphasized that the contribution of this research is primarily scientific in nature, specifically, to understand how a low-cost, intrinsically soft carbonaceous filler behaves within an ultrafine-grained aluminum matrix processed by severe plastic deformation, rather than to present an immediate industrial solution. The findings may provide a foundational basis for the future development of lightweight, cost-effective, and multifunctional composites, provided that the remaining challenges related to process scale-up and dispersion uniformity are addressed in subsequent studies.

2. Materials and Methods

2.1. Raw materials

Commercial AA1020 aluminum sheets with an initial thickness of 2 mm were used as the matrix material in this study. Rectangular specimens with dimensions of 80 × 20 mm were cut along the original rolling direction using a guillotine shear. The chemical composition of the sheets was determined by optical emission spectrometry (quantometric analysis) in accordance with ASTM E1251, and the results are summarized in Table 1.

Table 1. Chemical composition of AA1020 aluminum sheets determined by quantometry (wt.%)

Element	Zn	Si	Ni	Mn	Fe	Mg	Ti	Cr	Cu	Al
Spark1	0.0108	0.074	0.0032	0.0044	0.087	0.0012	0.0269	0.0074	0.0079	99.777
Spark2	0.0106	0.075	0.0032	0.0044	0.089	0.0012	0.0267	0.0062	0.0076	99.778
Mean	0.0107	0.0745	0.0032	0.0044	0.088	0.0012	0.0268	0.00675	0.00775	99.777

For the reinforcing phases, graphene oxide (GO) and industrial-grade carbon black (CB) were employed. Graphene oxide powder was synthesized from pyrolytic graphite (recovered from high-temperature metallurgical furnace residues) using a modified Hummer's method, following the procedure reported in Ref. [16]. The obtained GO had a lateral size of approximately 1–5 µm and a C:O atomic ratio of ~2.1 (according to the manufacturer's specification). The GO was dispersed in ethanol to prepare a suspension with a concentration of 1 g L^{-1} prior to deposition onto the aluminum sheets.

In addition, industrial-grade carbon black N115 (obtained from a local rubber industry supplier) was utilized as the alternative carbonaceous reinforcement. According to the manufacturer's technical specification, the N115 carbon black has an iodine adsorption number of 160±5 g/kg (ASTM D 1510), an oil absorption number of 115±5 cm^3/100g (ASTM D 2414), an ash content of ≤0.75% (ASTM D 1506), and a pour density of 345±30 kg/m^3 (ASTM D 1513). The primary feedstock for N115 carbon black production is hydrocarbon gas (e.g., natural gas) with a high methane and ethane content. This grade is commonly used in the rubber industry and is characterized by a colloidal morphology suitable for mechanical and electrical reinforcement [17].

Acetone (≥99.5% purity) and ethanol (≥99.8% purity) were purchased from commercial chemical suppliers and used as received. Copper wires (0.6 mm diameter in diameter) were commercially sourced.

2.2. Sample preparation

To assemble the initial sandwich structure, four holes were drilled at the corners of each sheet, allowing mechanical fixation using copper wires with a diameter of 0.6 mm. Prior to rolling, the sheet surfaces were degreased in acetone for 30 s and subsequently wire-brushed for 40 s using a steel brush mounted on a handheld mini-grinder to remove surface oxides and introduce controlled surface roughness. The brush wire diameter was 5 mm and the rotational speed was maintained at 750 rpm.

Brushing was performed following a consistent and predefined pattern for all samples, aligned with the rolling direction, such that continuous scratches were generated along the entire specimen length. The pattern consisted of unidirectional strokes along the rolling direction with approximately 50% overlap between adjacent passes to ensure uniform surface coverage.

For the GO-reinforced (GO/Al) and carbon black–reinforced (CB/Al) composite samples, approximately 2 mL of the corresponding suspension (1 g L^{-1} concentration in ethanol) was uniformly sprayed onto each sheet using an airbrush at a distance of 15 cm. This corresponds to approximately 2 mg of solid reinforcement (GO or CB) per sheet. Given the sheet dimensions (80 × 20 mm, an area of 16 cm^2 per side), this corresponds to a mass loading of approximately 0.125 $mg \cdot cm^{-2}$ per interface. The suspension was immediately sprayed onto the freshly brushed surfaces to ensure uniform coverage and minimize surface re-oxidation. The surface preparation tools are illustrated in Fig. 2.

The stacked sheets were tightly fastened using copper wires to prevent interlayer sliding during rolling. The time interval between surface preparation and rolling was minimized to reduce surface contamination and ensure effective interfacial bonding.

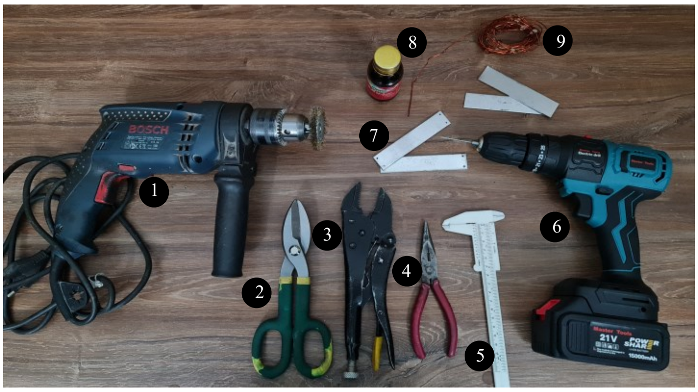

Fig. 2. Tools and materials used for surface preparation prior to ARB: (1) handheld mini-grinder with a steel wire brush (wire diameter: 5 mm, 750 rpm); (2) scissors for cutting rolled sheets; (3) pliers for holding sheets during drilling and brushing; (4) needle-nose pliers for tightening copper wires; (5) caliper for thickness measurement; (6) handheld drill for hole drilling at the sheet corners; (7) primary aluminum sheets (initial strips); (8) acetone for degreasing (30 s immersion); (9) copper wires (0.6 mm in diameter) for fastening the stacked sheets.

2.3. Accumulative roll bonding (ARB) process

Rolling was carried out using a laboratory-scale two-high rolling mill with roll diameter of 160 mm, a roll length of 220 mm, a motor power of 15 kW, and rotational speed of 46 rpm. Power transmission was provided through a gearbox-driven system. A thickness reduction of 50% per pass was imposed relative to the initial sandwich thickness.

For unreinforced aluminum samples, rolling was conducted both at room temperature (cold ARB) and under preheated conditions (hot ARB). In contrast, for GO- and carbon black–reinforced composites, only hot ARB was employed to ensure sufficient interfacial bonding between the layers. Preheating was performed in an electric furnace (Azarkoureh F11L 1320) at 380 °C for 4 min. The transfer time from furnace exit to the roll bite was approximately 15 s in order to minimize thermal loss prior to deformation.

After each pass, the rolled sheet was sectioned into two halves, surface preparation was repeated, the reinforcement suspension was re-applied, and the sheets were restacked to form a new sandwich configuration. The stacking sequence was arranged such that one half was oriented in the rolling direction and the other half in the reverse direction to promote strain homogenization. The maximum number of passes was five for cold ARB, seven for hot ARB, and four for both GO/Al and CB/Al composites. The pass limitation in cold rolling was primarily associated with edge cracking, whereas in hot rolling it was governed by excessive length reduction of the specimens.

Representative CB/Al composite sheets fabricated after up to four ARB passes are shown in Fig. 3. The figure confirms successful processing without edge cracking or delamination. Minor variations in length and width, as well as slight lateral deviations, are attributed to manual feeding without a side guide, a common characteristic of laboratory-scale ARB. Importantly, tensile specimens were extracted from the central uniform region of each sheet to ensure that the measured mechanical properties were not affected by these non-uniformities.

3. Results and Discussion

3.1. Mechanical behavior of ARB-processed sheets at room temperature

The mechanical response of the ARB-processed aluminum sheets was evaluated by uniaxial tensile testing. Tensile tests were performed using a universal testing machine (STM-250, Santam) following ASTM E8/E8M subsize specimen specifications at a crosshead speed of 2 mm·min^{-1} and room temperature (~22 °C). The specimens were wire-cut from the central region of the ARB-processed sheets along the rolling direction. The engineering stress–strain curves obtained after the first and fifth ARB passes, together with those of the initial AA1020 sheet, are presented in Fig. 4, while the corresponding quantitative mechanical parameters are summarized in Table 2.

Fig. 3. Aluminum–carbon black composite sheets after four ARB passes.

As shown in Fig. 4 and Table 2, ARB processing at room temperature results in a substantial enhancement of the ultimate tensile strength (UTS). The UTS increases from 136.9 MPa for the unprocessed aluminum to 249.3 MPa after the first pass and further to 259.4 MPa after the fifth pass, corresponding to an overall increase of approximately 89.5% relative to the base material. This pronounced strengthening is mainly attributed to the imposition of severe plastic deformation, progressive grain refinement, and the significant accumulation of dislocations during cumulative straining.

Conversely, the elongation to failure decreases markedly compared with the initial material, dropping from 26.9% to approximately 10.0% after the first pass. A slight recovery in ductility is, however, observed with further processing, as the elongation increases to 11.5% after the fifth pass. This trend suggests a partial restoration of deformability at higher accumulated strains, which can be associated with microstructural homogenization and the gradual improvement of the interlayer bonding quality. It is important to note that the edge cracking observed in cold ARB after higher passes occurs only at the sheet edges, while tensile specimens were extracted from the central crack-free region. Therefore, the measured increase in elongation reflects the true evolution of bulk deformability and is not contradicted by the presence of edge cracks, which remain a separate processing limitation.

To evaluate the combined contribution of strength and ductility, the strain energy density (SED) was derived from the tensile curves. Despite the pronounced strengthening, the SED decreases from 34.2 MJ m^{-3} for the unprocessed aluminum to 19.8 and 21.9 MJ m^{-3} after the first and fifth passes, respectively. Nevertheless, the approximately 10.6% increase in SED between the first and fifth passes indicates a relative improvement in the balance between strength and ductility with an increasing number of ARB cycles.

From a microstructural standpoint, the progressive evolution of mechanical performance can be attributed to continuous changes in grain morphology and grain boundary characteristics. The ARB process imposes extremely high plastic strains, transforming the initial coarse-grained microstructure into an ultrafine-grained (UFG) structure with a more homogeneous through-thickness distribution [18, 19]. Grain refinement, accompanied by an increased fraction of grain boundaries, enhances the resistance to dislocation motion and thus contributes to strengthening [20]. In parallel, the elevated dislocation density and the formation of stable dislocation substructures promote effective strain hardening at the early stages of deformation [19]. With an increasing number of passes, the growing fraction of high-angle grain boundaries (HAGBs) and the gradual weakening of the dominant crystallographic texture facilitate a more uniform strain distribution and alleviate localized stress concentrations, leading to a partial recovery of ductility and enhanced energy absorption capability [21]. Moreover, the multilayer architecture inherent to the ARB process and the progressive improvement of interfacial bonding can suppress strain localization and delay crack initiation and propagation, thereby promoting a more favorable trade-off between strength and ductility. Similar concurrent trends have been reported for ultrafine-grained aluminum systems, underscoring the effectiveness of ARB in tailoring microstructure and mechanical performance simultaneously [22].

Table 2. Mechanical properties of ARB-processed aluminum sheets after the first and fifth passes at room temperature, compared with the initial AA1020 sheet

Tested sheet	UTS (MPa)	Elongation (%)	SED (MJ/m³)
Unprocessed Al	136.9	26.9	34.2
Al-ARB (Cold)-P1	249.3	10	19.8
Al-ARB (Cold)-P5	259.4	11.5	21.9

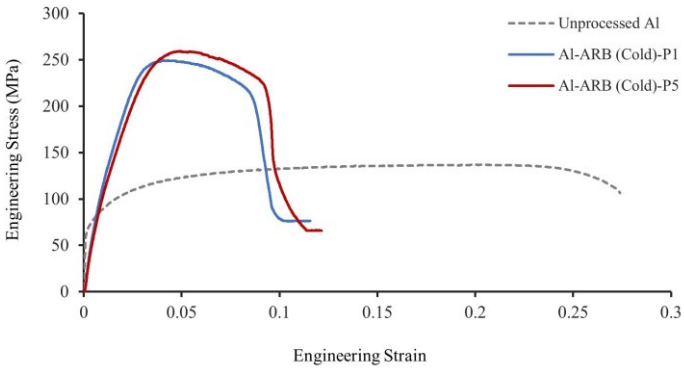

Fig. 4. Engineering stress–strain curves of AA1020 sheets processed by ARB after the first and fifth passes at room temperature, compared with the initial material.

3.2. Effect of thickness reduction on mechanical properties

To evaluate the influence of the imposed strain level, uniaxial tensile tests were performed on ARB-processed aluminum sheets subjected to different thickness reduction ratios (Fig. 5 and Table 3). The results indicate that increasing the thickness reduction from 50% to 62% leads to a noticeable decrease in ultimate tensile strength (UTS), which can be attributed to the onset of microstructural instabilities and/or degradation in interlayer bonding quality. Upon further increasing the thickness reduction to 68%, no significant additional improvement in strength is observed, and only a marginal increase is recorded.

From a processing perspective, higher single-pass reductions impose larger strain gradients and higher interfacial shear stresses. These conditions promote local damage accumulation, interface decohesion, and heterogeneous strain localization, which ultimately limit the load transfer capability and mechanical stability of the laminate. In addition, excessive thickness reduction may intensify surface oxidation and frictional heating effects, potentially impairing interfacial bonding quality.

Considering the combined balance among mechanical strength, ductility, and process stability, a thickness reduction ratio of 50% was selected as the optimal condition for subsequent experiments.

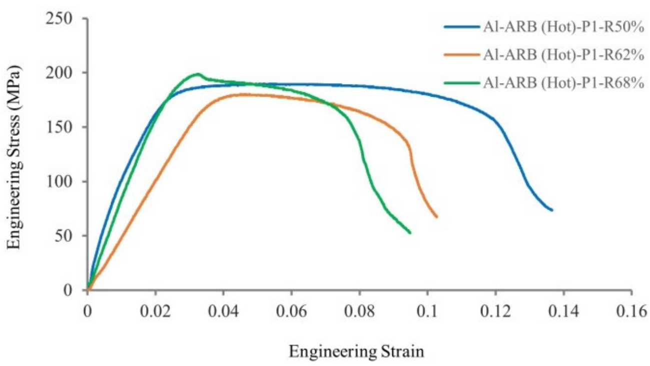

Fig. 5. Engineering stress–strain curves of ARB-processed aluminum sheets under preheated conditions with different thickness reduction ratios.

Table 3. Mechanical properties of ARB-processed aluminum sheets after one pass with different thickness reduction ratios

Tested Sheet	UTS (MPa)	Elongation (%)	SED (MJ/m³)
Reduction 50%	189.9	13.8	22.1
Reduction 62%	180.18	11.05	14.30
Reduction 68%	198.87	9.47	13.77

3.3. Effect of preheating on the ARB process

To elucidate the influence of processing temperature on mechanical behavior and interfacial bonding, the specimens were preheated to 380 °C in a furnace and immediately subjected to rolling. The engineering stress–strain responses of cold- and preheated-ARB samples after the first pass are compared in Fig. 6, and the corresponding mechanical properties are summarized in Table 4.

Preheating results in an approximately 23.8% reduction in UTS, accompanied by an increase of about 38% in elongation and 11.6% in SED. This behavior is attributed to the activation of thermally assisted deformation mechanisms, including dynamic recovery, a reduced work-hardening rate, and enhanced dislocation mobility at elevated temperatures. The increase in SED indicates that the beneficial effects of improved ductility outweigh the reduction in strength under preheated conditions.

The hot ARB process was successfully extended to seven passes. The corresponding stress–strain curves for passes 1, 5, and 7 are presented in Fig. 7, and the quantitative results are listed in Table 5. With an increasing number of passes under preheated conditions, the UTS exhibits a mild decreasing trend, whereas both elongation and SED progressively increase. This trend reflects the dominance of thermally activated softening mechanisms over strain hardening, as well as the occurrence of dynamic recovery and the possible onset of partial recrystallization. In addition, the relaxation of residual stresses during warm deformation facilitates continued processing to higher passes. By contrast, cold ARB was limited to five passes due to the formation of edge cracking, which restricted the production of defect-free sheets.

Table 4. Mechanical properties of ARB-processed aluminum sheets under cold and preheated conditions after the first pass.

Tested sheet	UTS (MPa)	Elongation (%)	SED (MJ/m³)
Al-ARB (Cold)-P1	249.3	10	19.8
Al-ARB (Hot)-P1	189.9	13.8	22.1

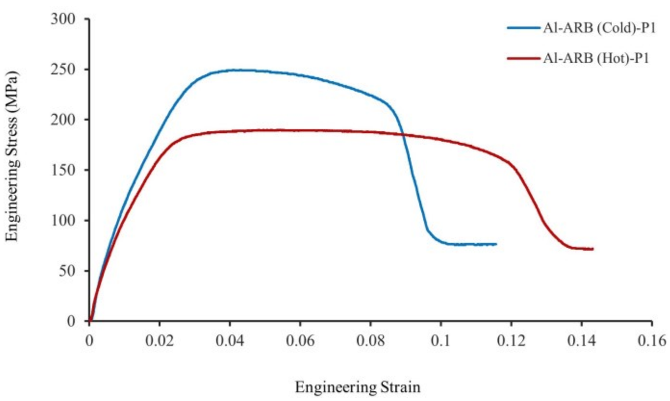

Fig. 6. Comparison of engineering stress–strain curves of AA1020 sheets processed by ARB under cold and preheated conditions after the first pass.

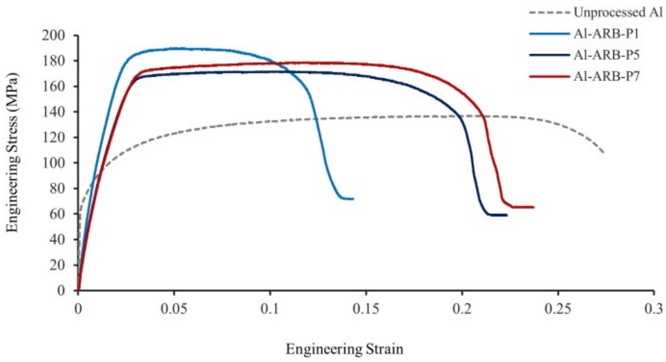

Fig. 7. Engineering stress–strain curves of AA1020 sheets processed by ARB under preheated conditions after the first, fifth, and seventh passes, compared with the initial material.

Table 5. Mechanical properties of AA1020 sheets processed by ARB under preheated conditions after the first, fifth, and seventh passes

Tested Sheet	UTS (MPa)	Elongation (%)	SED (MJ/m³)
Unprocessed Al	136.9	26.9	34.2
Pass 1	189.9	13.8	22.1
Pass 5	171.5	21.5	32.7
Pass 7	178.8	22.7	35.9

3.4. Incorporation of carbonaceous and graphene-based reinforcements

In recent years, graphene-derived reinforcements have attracted considerable attention for the development of aluminum matrix composites owing to their exceptional strength-to-weight ratio, high thermal conductivity, and mechanical stability [23]. Nevertheless, the high production cost and processing complexity of graphene and its derivatives impose significant economic constraints on large-scale industrial implementation. In this context, low-cost carbonaceous reinforcements such as carbon black represent a promising alternative for fabricating economically viable composites with acceptable mechanical performance.

In the present study, GO/Al and CB/Al composites were fabricated by spraying the reinforcement suspensions onto the aluminum surfaces followed by ARB processing under preheated conditions. The engineering stress–strain curves obtained after the first and third passes are presented in Fig. 8, and the corresponding mechanical properties are summarized in Table 6.

As evidenced in Table 6, both reinforcement systems lead to a pronounced increase in strength after the first ARB pass compared with the unprocessed aluminum. The UTS reaches 198.8 MPa for CB/Al-ARB-P1 and 208.2 MPa for GO/Al-ARB-P1, indicating comparable strengthening efficiency at the early stage of deformation. This observation confirms that even an initial dispersion of carbon black particles is capable of providing effective strengthening in the aluminum matrix through mechanisms such as dislocation pinning and localized load transfer.

With an increasing number of passes (up to the third pass), the mechanical response of the two composite systems diverges. In the GO/Al composite, although the UTS decreases slightly by approximately 2.9%, the elongation and SED increase by about 23% and 28.5%, respectively, reflecting enhanced deformation stability and improved damage tolerance. This behavior can be attributed to the relatively stable dispersion of GO nanosheets, stronger interfacial bonding, and their effectiveness in mitigating stress concentration and delaying microcrack initiation.

In contrast, the CB/Al composite exhibits a noticeable reduction in UTS, elongation, and SED at the third pass. This degradation is attributed to the intrinsic characteristics of carbon black particles and their limited microstructural stability under high cumulative strain. The high surface energy and relatively weaker interfacial bonding between carbon black and the aluminum matrix promote particle re-agglomeration during severe rolling deformation, leading to the formation of local stress concentration zones, impaired load transfer efficiency, and an increased tendency for interfacial debonding. At the macroscopic scale, these effects reduce the continuity of the load-bearing network and result in deteriorated tensile performance at higher passes, despite the potential for local hardness enhancement.

Nevertheless, even after three ARB passes, the UTS of the CB/Al composite remains approximately 40% higher than that of the unprocessed aluminum, highlighting carbon black as a promising low-cost reinforcement for aluminum matrix composites.

For a direct comparison of the reinforcement effects at the first pass, Fig. 9 and Table 7 show that the incorporation of GO increases the UTS by approximately 9.6%, whereas carbon black provides an increase of about 4.7% relative to the unreinforced hot-ARB aluminum. Conversely, both reinforcements lead to a reduction in elongation, with decreases of approximately 18% and 17% for GO and CB, respectively. These results reflect the classical strength–ductility trade-off commonly observed in particle-reinforced metal matrix composites.

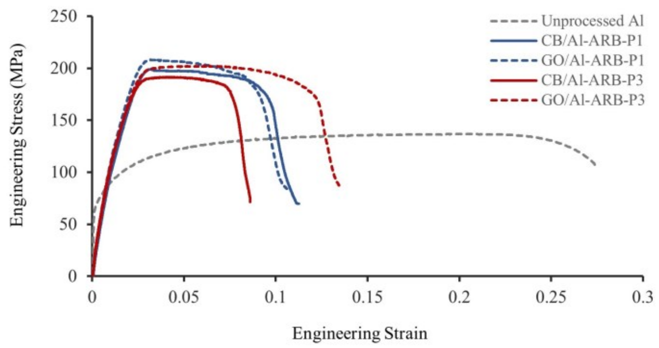

Fig. 8. Engineering stress–strain curves of GO/Al and CB/Al composites processed by ARB under preheated conditions after the first and third passes, compared with the unprocessed aluminum.

Table 6. Mechanical properties of GO/Al and CB/Al composites fabricated by ARB under preheated conditions after the first and third passes

Tested Sheet	UTS (MPa)	Elongation (%)	SED (MJ/m³)
Unprocessed Al	136.9	26.9	34.2
CB/Al-ARB-P1	198.8	11.4	18.5
GO/Al-ARB-P1	208.2	11.3	18.6
CB/Al-ARB-P3	191.6	8.6	13.8
GO/Al-ARB-P3	202.2	13.9	23.9

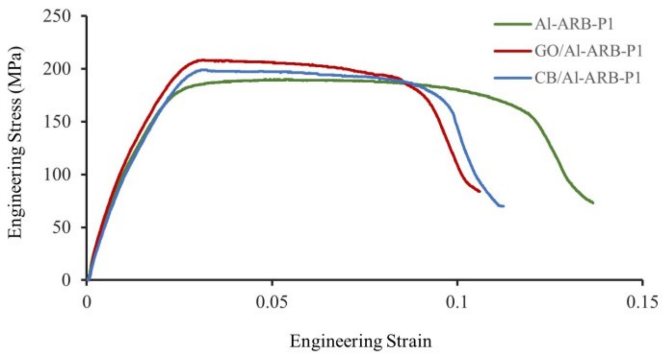

Fig. 9. Engineering stress–strain curves of ARB-processed aluminum sheets reinforced with graphene oxide and carbon black after the first pass.

Table 7. Mechanical properties of ARB-processed sheets after the first pass for different reinforcement conditions

Tested Sheet	UTS (MPa)	Elongation (%)	SED (MJ/m³)
Al-ARB-P1	189.9	13.8	22.1
CB/Al-ARB-P1	198.8	11.4	18.5
GO/Al-ARB-P1	208.2	11.3	18.6

Overall, the results demonstrate that although graphene oxide provides superior mechanical stability and toughness retention at higher cumulative strains, carbon black delivers comparable early-stage strengthening performance at a substantially lower material cost and with more favorable industrial feasibility. This combination renders carbon black an attractive candidate for cost-sensitive and scalable engineering applications.

3.5. Microhardness

To evaluate the influence of carbonaceous reinforcements on the hardness behavior of aluminum matrix composites, the average Vickers microhardness of the composite specimens was compared with that of aluminum sheets processed by ARB under identical preheated conditions and using identical processing routes. Specimens were sectioned from the transverse cross-section of the sheets, mounted using hot compression mounting, mechanically ground and polished, and then subjected to hardness measurements along the mid-thickness line of the cross-section. For each specimen, ten indentations were performed and the average value was reported. Microhardness tests were conducted using a Jenus microhardness tester equipped with a diamond pyramidal indenter under an applied load of 50 gf and a dwell time of 12 s.

The evolution of the average microhardness of GO/Al and CB/Al composites in comparison with preheated ARB-processed aluminum is presented in Fig. 10.

As shown in Fig. 10, the unreinforced aluminum specimen exhibits an approximately 2.8% reduction in hardness after the first preheated ARB pass relative to the initial sheet. This reduction can be attributed to the activation of thermal recovery processes, a decrease in dislocation density, and partial suppression of work hardening at elevated temperature. With an increasing number of passes, the hardness evolution of the unreinforced sample is governed primarily by the competition between grain refinement induced by severe plastic deformation and thermal softening associated with recovery and dynamic recrystallization.

In contrast, the presence of carbonaceous reinforcements leads to a pronounced increase in hardness relative to the unreinforced samples at all passes. In the first pass, the hardness of GO/Al and CB/Al composites increases by approximately 4.1% and 6.1%, respectively, compared with the preheated ARB aluminum, confirming the effective role of reinforcement

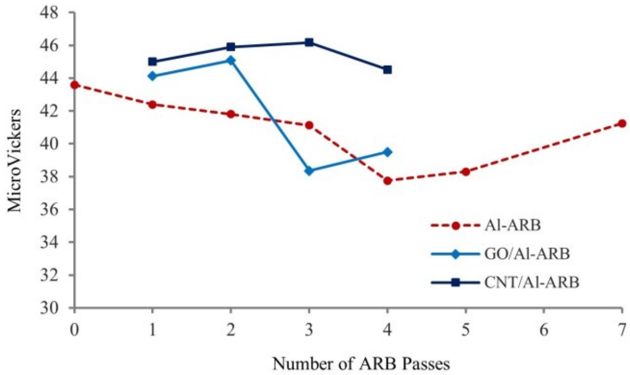

Fig. 10. Variation of the average microhardness through the thickness of GO/Al and CB/Al samples processed by preheated ARB at different passes, compared with unreinforced aluminum.

particles in restricting dislocation motion and enhancing resistance to plastic deformation. This improvement can be attributed to the combined contribution of several strengthening mechanisms, including particle strengthening (Orowan looping), localized load transfer to the stiffer particles, and increased dislocation density in the vicinity of particle–matrix interfaces.

A notable observation is the distinct behavior of CB/Al compared with GO/Al at higher passes. The maximum hardness enhancement in CB/Al is achieved at the third pass, reaching approximately 12.3% relative to the unreinforced aluminum, whereas the GO/Al composite exhibits a pronounced decline in hardness at the same pass.

The higher hardness of CB/Al relative to GO/Al can be rationalized by fundamental differences in particle morphology, as documented in the literature for carbon black [17] and graphene oxide [9-13]. Carbon black particles, owing to their ultrafine size, high number density, quasi-spherical morphology, and lower tendency to form continuous planar networks, can be more uniformly dispersed within the aluminum matrix and generate a larger population of effective obstacles to dislocation motion. This promotes dispersion strengthening and enhances local hardness. Since microhardness measurements probe a very limited material volume, the dislocation-blocking effect of finely dispersed particles remains dominant even in the presence of moderate agglomeration. This interpretation is qualitatively supported by our FESEM observations (Section 3.7); however, quantitative analyses of the the particle size distribution are recommended for future work to further validate this claim.

Conversely, graphene-based reinforcements, due to their platelet-like morphology, tendency toward wrinkling, interlayer sliding, and localized agglomeration, may exhibit reduced efficiency in dislocation pinning at the local scale, particularly at higher ARB passes under preheated conditions. Moreover, under elevated temperature processing, graphene derivatives are more susceptible to local structural degradation, surface oxidation, or interfacial debonding compared with carbon black, which can weaken load transfer efficiency and diminish the effective strengthening contribution. In contrast, the higher thermal stability and more isotropic mechanical response of carbon black favor the preservation of its dislocation-blocking capability even at higher cumulative strains.

The relative decrease in hardness at higher passes for both composite systems can be attributed to the increasing dominance of thermal softening and dynamic recrystallization over strain-hardening mechanisms. Nevertheless, the magnitude of the hardness degradation is less pronounced in CB/Al, indicating the superior mechanical stability of this system during preheated ARB processing.

It should be noted that all hardness measurements were performed along the mid-thickness line of the cross-section to obtain representative bulk hardness. Future work could include through-thickness hardness mapping (perpendicular to the sheets) to assess the layer-by-layer hardness variation.

3.6. Electrical resistance

To evaluate the electrical conduction behavior of the aluminum-based composites and to assess the effectiveness of carbon black as a reinforcement in comparison with graphene oxide–reinforced composites, electrical resistance measurements were performed on sheet specimens. Since electrical conductivity is a critical functional parameter in many engineering applications of aluminum and metal matrix composites (MMCs), the coupled analysis of microstructural evolution and electrical response is essential for assessing the industrial applicability of these materials. Fig. 11 illustrates the variation in the electrical resistance of the composite sheets and ARB-processed samples in comparison with the unprocessed aluminum.

As expected, the unprocessed aluminum exhibits the lowest electrical resistance (0.076 Ω), which can be attributed to its low density of crystallographic defects, the absence of severely deformed grain boundaries, and the minimal presence of surface and interfacial oxide layers. The imposition of severe plastic deformation during the ARB process significantly increases the

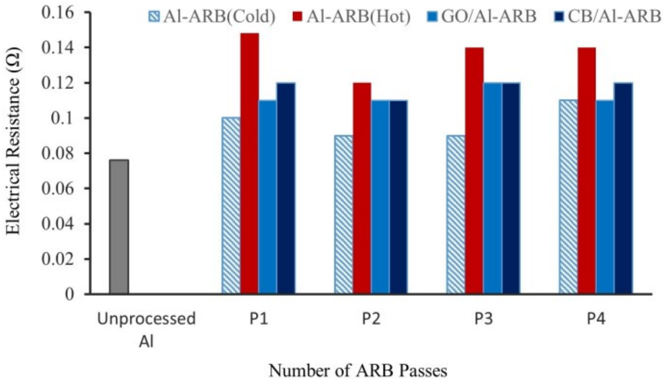

Fig. 11. Electrical resistance variation of CB/Al and GO/Al composites compared with unprocessed aluminum and ARB-processed sheets under cold and preheated conditions.

dislocation density, refines the grain structure, and introduces a large number of interlayer interfaces, all of which act as effective electron-scattering centers and thereby increase the electrical resistance.

With an increasing number of ARB passes, in addition to the progressive accumulation of lattice defects, the growth and thickening of oxide layers at interlayer interfaces emerge as electrically resistive barriers, further intensifying the upward trend in the electrical resistance.

The results in Fig. 11 indicate that the specimens processed by ARB under preheated conditions exhibit systematically higher electrical resistance than those processed under cold ARB conditions. Although elevated temperature may partially mitigate work hardening and reduce the steady-state dislocation density through recovery mechanisms, the accelerated formation and growth of surface and interfacial oxide layers under preheating conditions become the dominant factor governing the electrical response and thus lead to a net increase in resistance. This observation suggests that, under preheated ARB conditions, oxide-related interfacial barriers rather than deformation-induced defects represent the primary rate-controlling mechanism for electrical conductivity.

The incorporation of both graphene oxide and carbon black reinforcements results in a noticeable reduction in electrical resistance compared with the unreinforced preheated ARB aluminum sheets, and this trend is consistently observed at all processing passes (Fig. 11). The maximum reduction occurs at the first pass, where the electrical resistance decreases by approximately 26.7% and 20% for the GO/Al and CB/Al composites, respectively. This behavior can be attributed to improved interlayer bonding quality, the suppression of local interfacial separations, and enhanced metallurgical continuity, which collectively provide more effective conductive pathways for electron transport. Similar trends have been reported in graphene-reinforced aluminum composites containing low graphene contents, where reduced interfacial defects and improved interlayer bonding were identified as the primary contributors to enhanced electrical conductivity [24].

A quantitative comparison of the data in Table 9 reveals that the difference in electrical resistance between the CB/Al and GO/Al composites remains below 10% across all ARB passes. This limited discrepancy indicates that, despite the intrinsically lower electrical conductivity of carbon black relative to graphitic or graphene-like structures, the favorable dispersion of the particles within the aluminum matrix, the absence of continuous insulating networks, and the preservation of interfacial integrity effectively prevent any substantial degradation in electrical performance. From an application-oriented perspective, this result is particularly significant, as it demonstrates that carbon black, as a cost-effective reinforcement, can deliver electrical performance comparable to that of graphene oxide while offering clear economic and processing advantages, thereby representing a viable alternative for the development of aluminum matrix composites.

3.7. FESEM characterization

To establish the structure–property relationships in the

ARB-processed composites, detailed microstructural characterization was performed on the cross-sections of GO/Al and CB/Al specimens after the third ARB pass using field-emission scanning electron microscopy (FESEM). Fig. 12 presents FESEM micrographs of the GO/Al composite at multiple magnifications. At low magnification (Fig. 12(a)), a well-bonded multilayer structure is evident with continuous aluminum layers and no macroscopic delamination or large-scale voids. At intermediate magnifications (Figs. 12(b–c)), GO nanosheets appear as thin, fragmented, and flattened platelets aligned parallel to the rolling direction, forming a characteristic mosaic-like pattern. This morphology results from the severe shear deformation and repeated folding during ARB, consistent with the exfoliation and alignment of 2D reinforcements under high strain. The Higher-magnification (Fig. 12(d)) reveals fine intralayer cracks within individual GO sheets, which are attributed to the nature of graphene oxide under intense in-plane shear. Importantly, the Al/GO interfaces remain sharp and well-adhered, with no detectable interfacial voids, debonding, or reaction products.

Table 8. Electrical resistance of CB/Al composites compared with preheated ARB-processed aluminum and GO/Al composites (Percentage variation of CB/Al relative to each reference sample is given in parentheses)

Processing pass	CB/Al composite (Ω)	Preheated ARB Al (Ω)	GO/Al composite (Ω)
Pass 1	0.12	0.15 (−20.0%)	0.11 (+9.0%)
Pass 2	0.11	0.12 (−8.3%)	0.11 (0.0%)
Pass 3	0.12	0.14 (−14.3%)	0.12 (0.0%)
Pass 4	0.12	0.14 (−14.3%)	0.11 (+9.0%)

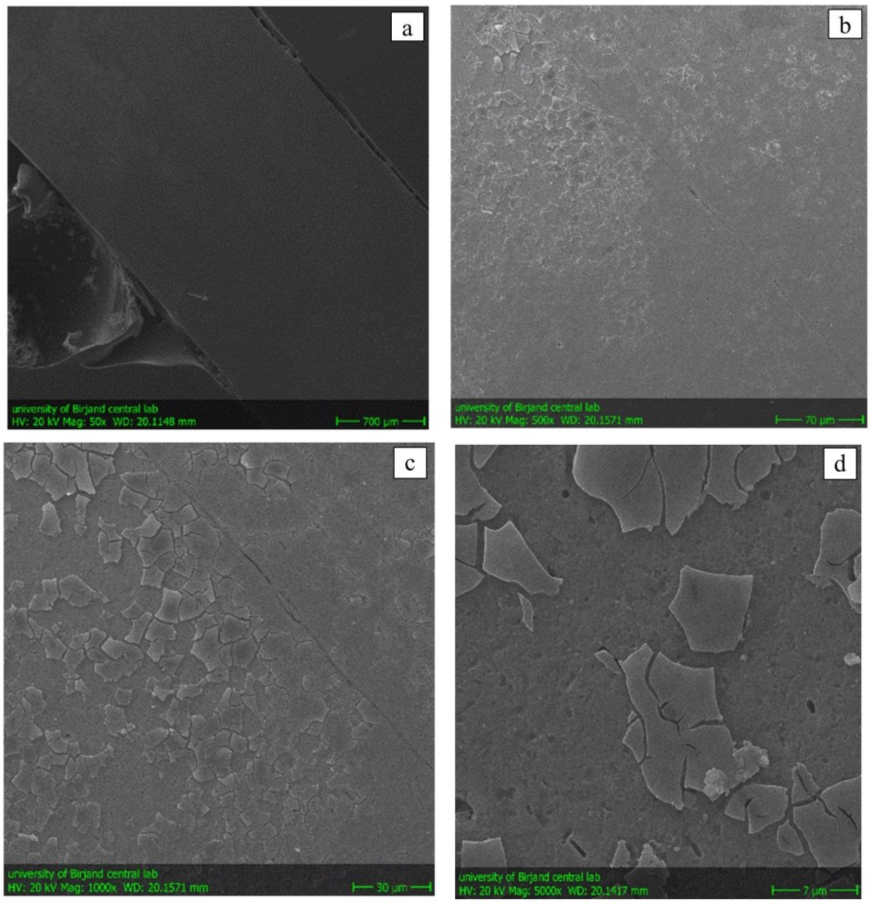

Fig. 12. FESEM images of the cross-section of the GO/Al composite after the third ARB pass at various magnifications.

This microstructure is consistent with the measured mechanical and electrical properties at the third pass. The presence of flattened and fragmented GO sheets without interfacial debonding maintains good adhesion between the Al/GO layers. This interlaminar cohesion results in an increase in the toughness of the GO/Al sample at the third pass compared to the first pass (SED increased from 18.6 to 23.9 MJ/m³). Furthermore, although the presence of GO increases electrical resistance relative to pure aluminum, the absence of observable agglomeration and the preservation of matrix continuity keep the resistance lower than that of the unreinforced ARB-processed aluminum sheets.

Fig. 13 shows the corresponding micrographs for the CB/Al composite. In contrast to the platelet morphology of GO, carbon black particles produce a distinctly different distribution. At low-to-intermediate magnifications (Figs. 13(a–c)), the aluminum matrix appears relatively homogeneous and featureless, with carbon black clusters remaining below the resolution limit of SE imaging at these scales. At high magnification (Fig. 13(d)), localized nanoscale heterogeneity and grain boundary pinning effects become visible. No large agglomerates (>1 μm) or significant porosity were observed, although occasional small clusters were present, indicating partial re-agglomeration during processing.

This microstructure is fully consistent with the mechanical behavior of CB/Al. The uniform distribution of CB nanoparticles within the aluminum matrix leads to more effective dislocation pinning and, consequently, higher hardness of CB/Al compared with GO/Al (Fig. 10). On the other hand, the refined distribution of GO sheets within the aluminum matrix enhances deformation energy absorption and increases the toughness and tensile strength of GO/Al (Table 6). In other words, CB/Al is harder, whereas GO/Al exhibits superior tensile and ductile behavior, reflecting the different mechanisms governing hardness versus toughness in the two composites. For CB/Al, the decrease in toughness and UTS at the third pass relative to the first pass can be attributed to local agglomerations or fine discontinuities observed in Fig. 13(d). From an electrical perspective, the good continuity of the aluminum phase preserves conductive pathways, and the difference in electrical conductivity between CB/Al and GO/Al remains below 10% (Table 8).

3.8. Comparison with literature

To provide a broader context for the present findings, the results of this study are compared with recent reports on ARB-processed aluminum matrix composites reinforced with carbonaceous nanomaterials (Table 9).

Comparison of strength improvement: Singh et al. [25] reported a 14.15% increase in yield strength for Al 6061/GO composite (0.2 wt.% GO) after 5 ARB passes compared to unreinforced ARB-processed Al 6061. Yang et al. [26] reported a 14.1% increase in ultimate tensile strength for Al 5052/graphene composite (0.083 vol.% graphene) after 8 ARB cycles. Our GO/Al composite (≈0.01-0.02 wt.% GO) showed a 9.6% increase in UTS at pass 1, while our CB/Al composite showed a 4.7% increase. Considering that our reinforcement content is approximately 10-20 times lower than that used by Singh et al. [25] and comparable to Yang et al. [26], the observed improvements are within the expected range. The lower strength increase in our CB/Al composite is consistent with the intrinsically softer nature of carbon black compared with graphene derivatives.

Comparison of hardness improvement: Yang et al. [26] reported the highest hardness increase (29.4% at 8 cycles), followed by Singh et al. [25] (17.23% at 5 passes). Our CB/Al composite showed a 6.1% increase in hardness at pass 1, which is higher than our GO/Al composite (4.1%). This observation confirms that CB particles, despite their lower reinforcement efficiency in tensile strength, provide effective local dislocation pinning and contribute to surface hardness.

Comparison of elongation trend: Singh et al. [25] reported a 20.6% decrease in elongation for their GO/Al composite (0.2 wt.% GO) compared to unreinforced ARB-processed Al. Our CB/Al and GO/Al composites showed decreases of 17.4% and 18.1%, respectively, which are slightly lower than Singh et al. [25]. Interestingly, Yang et al. [26] reported an increase in elongation (47.5%) for their graphene/Al composite, which is exceptional and attributed to the in situ exfoliation of graphene layers and interlayer slip behavior. This suggests that under optimized conditions (very low reinforcement content, specific processing parameters), carbonaceous reinforcements can simultaneously enhance strength and ductility.

Despite the modest strength improvements in our study (due to the very low reinforcement content used for cost considerations), the performance of our composites is within the expected range based on literature. The higher hardness of CB/Al compared to GO/Al, even at very low reinforcement content, highlights the potential of carbon black as a cost-effective reinforcement for applications requiring high surface hardness. Future work with higher CB/GO contents and optimized processing parameters may further improve the mechanical performance.

Table 9. Comparison of composite properties and resulting mechanical properties between literature studies and the present work (CB/Al and GO/Al)

Parameter	Singh et al. (2026) [25]	Yang et al. (2025) [26]	This study (CB/Al)	This study (GO/Al)
Matrix alloy	Al 6061	Al 5052	AA1020	AA1020
Reinforcement content	0.2 wt.% (high)	0.083 vol.% (very low)	~0.01-0.02 wt.% (very low)	~0.01-0.02 wt.% (very low)
ARB passes	5 passes	8 passes	1 pass	1 pass
UTS/YS increase*	14.15% (YS)	14.1% (UTS)	4.7% (UTS)	9.6% (UTS)
Hardness increase*	17.23%	29.4%	6.1%	4.1%
Elongation trend*	Decreased (20.6%)	Increased (47.5%)	Decreased (17.4%)	Decreased (18.1%)

**Relative to unreinforced ARB-processed Al of the same alloy at the same number of passes*

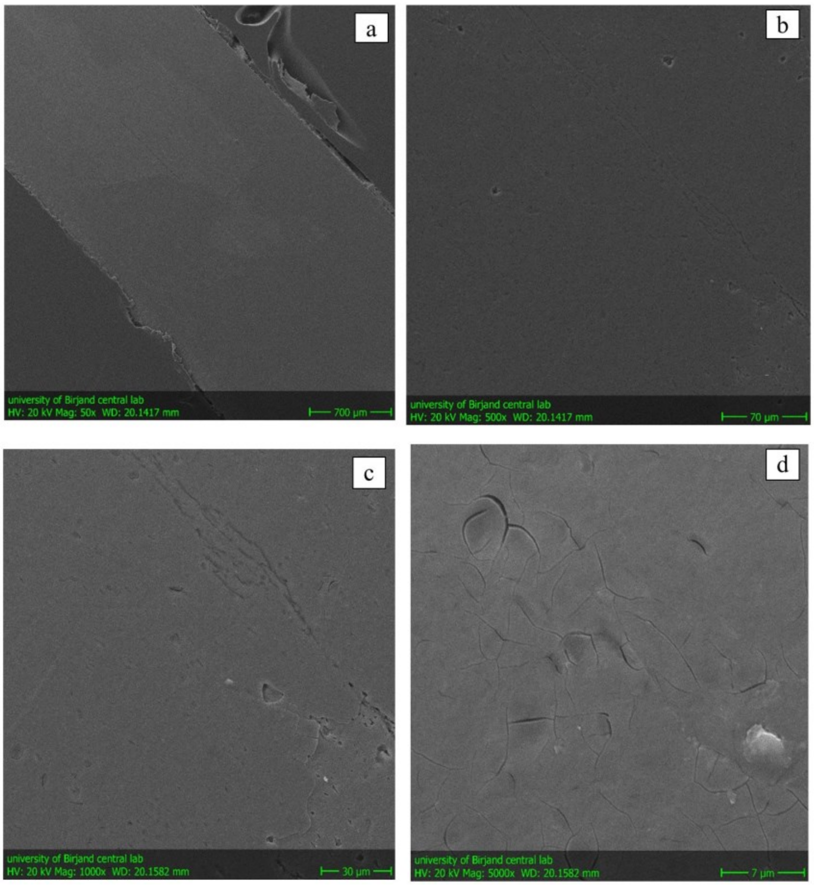

Fig. 13. FESEM images of the cross-section of the CB/Al composite after the third ARB pass at various magnifications.

4. Conclusions

In this study, the feasibility of employing carbon black (CB) as a low-cost and industrially scalable reinforcement for aluminum matrix composites fabricated by accumulative roll bonding (ARB) under preheated conditions was investigated. The mechanical behavior, microhardness, and electrical resistance of CB/Al composites were compared with unprocessed aluminum, cold- and preheated-ARB aluminum sheets, and graphene oxide reinforced composites (GO/Al). The main findings can be summarized as follows:

(1) **Effect of ARB and preheating:** Cold ARB significantly increased the ultimate tensile strength (up to ~90%) at the expense of ductility due to severe strain hardening and grain refinement. Preheating reduced strength but improved ductility and enabled stable processing at higher passes without edge cracking.

(2) **Strengthening effect of CB:** The introduction of carbon black during the first preheated pass increased the ultimate tensile strength by 4.7% compared with the unreinforced preheated sheet (from 189.9 MPa to 198.8 MPa). The total increase relative to initial aluminum is 45.2%, the majority of which (≈40.5%) is attributed to work hardening and grain refinement from the ARB process itself.

(3) **Mechanical stability at higher strains:** With increasing accumulated strain, CB/Al exhibited degradation in strength and ductility, mainly attributed to particle re-agglomeration and limited interfacial bonding.

(4) **Microhardness behavior:** Carbon black consistently increased microhardness at all passes, with a maximum increment of ~12.3%, exceeding that of GO/Al, although this local strengthening was not fully translated into global tensile performance.

(5) **Electrical performance:** Both CB and GO reduced electrical resistance compared with unreinforced sheets, with a maximum reduction of ~20% for CB/Al in the first pass, and a difference of less than 10% between the two reinforcements. Overall, although GO/Al exhibits superior mechanical stability and toughness at higher accumulated strains, CB/Al delivers competitive early-stage mechanical and electrical performance together with higher local hardness. Considering the substantially lower cost, ease of supply, and relative scalability potential compared to other reinforcements of carbon black, it represents a practical reinforcement option for applications where performance-to-cost efficiency is the primary design criterion. To further enhance the performance of CB/Al composites at higher ARB passes, future work should focus on particle surface modification, improved dispersion strategies, precise control of preheating temperature, and the development of hybrid reinforcement systems.

Acknowledgments

This work has been supported by the Center for International Scientific Studies & Collaboration (CISSC), Ministry of Science, Research and Technology of Iran.

Authors' contributions

S. E. Eftekhari Shahri: Conceptualization, Methodology, Data analysis, Supervision, Project administration, Writing- original draft. Led the overall research design and coordinated the experimental framework

S. E. Fatemi: Experimental Investigation, Sample preparation, Mechanical testing, Electrical conductivity measurements, Data collection

A. Saghafi: Supervision, Data interpretation, Results validation, Writing - review & editing

Y. Yaghoubinezhad: Data analysis, Materials behavior and microstructural interpretation, Conceptual understanding of the study, Carbon material Preparation, experimental supervision, Writing - review & editing.

A. M. Dimiev: Scientific consultation on graphene and carbon material preparation, Microstructural evaluation, Manuscript reviewing and final editing

Conflict of interest

The authors declared no potential conflicts of interest with respect to the research, authorship and/or publication of this paper.

Funding

No external funds were disbursed for this study; the work was conducted under a research agreement with CISSC (MSRT, Iran).

Data availability

The datasets generated and analyzed during the current study are available from the corresponding author upon reasonable request

5. References

[1] Trajano, A. A., de Oliveira, L. R., da Costa, M. E. L., da Costa, P. R., & dos Santos, R. F. (2024). Accumulative roll bonding (ARB) and cross accumulative roll bonding (CARB) in aluminum: A review. *Materials Science and Technology*, 1-27. https://doi.org/10.1177/02670836241303270

[2] Ramkumar, K., Senthil, P., Ananth, S., & Arul, K. (2024). Development of aluminum matrix composites through accumulative roll bonding: A review. *Journal of Materials Science*, *59*(20), 8606-8649. https://doi.org/10.1007/s10853-024-09902-1

[3] Ebrahimi, M., & Wang, Q. (2022). Accumulative roll-bonding of aluminum alloys and composites: An overview of properties and performance. *Journal of Materials Research and Technology*, *19*, 4381-4403. https://doi.org/10.1016/j.jmrt.2022.06.045

[4] Dong, H., Chen, X., Li, Y., Zhang, Z., Wang, S., & Liu, J. (2025). Interface-dominated microstructure development and mechanical and electrical properties of Al/Cu multilayered composites prepared via multicomponent accumulative roll bonding. *Journal of Alloys and Compounds*, *1017,* 179149. https://doi.org/10.1016/j.jallcom.2025.179149

[5] Dehghan, M., Hosseini, M., Ghasemi, H. M., & Poursalehi, R. (2020). Effect of inter-cycle heat treatment in accumulative roll-bonding (ARB) process on planar isotropy of mechanical properties of AA1050 sheets. *Transactions of Nonferrous Metals Society of China*, *30*(9), 2381-2393. https://doi.org/10.1016/S1003-6326(20)65377-1

[6] Hausöl, T., Höppel, H. W., & Göken, M. (2010). Tailoring materials properties by accumulative roll bonding. *Advanced Engineering Materials*, *12*(8), 740-746. https://doi.org/10.1002/adem.201000045

[7] Kang, H., Kim, J., & Lee, C. (2007). A combined texture and FEM study of strain states during roll-cladding of five-ply stainless steel/aluminum composites. *Materials Science and Engineering: A*, *452,* 347-358. https://doi.org/10.1016/j.msea.2006.10.089

[8] Yazdani, A., & Salahinejad, E. (2011). Evolution of reinforcement distribution in Al–B_4C composites during accumulative roll bonding. *Materials & Design, 32*(6), 3137-3142. https://doi.org/10.1016/j.matdes.2011.02.017

[9] Yao, G., Wu, Y., Huang, J., & Zhang, L. (2016). Cu/C composites with a good combination of hardness and electrical conductivity fabricated from Cu and graphite by accumulative roll-bonding. *Materials & Design*, *110*, 124-129. https://doi.org/10.1016/j.matdes.2016.07.078

[10] Chen, Z. H., Zhao, X. D., Chen, D., & Li, X. B. (2021). GNPs/Al nanocomposites with high strength and ductility and electrical conductivity fabricated by accumulative roll-compositing. *Rare Metals*, *40*(9), 2593-2601. https://doi.org/10.1007/s12598-020-01634-8

[11] Tiwari, J. K., Mandal, A., Sathish, N., Manna, R., & Chakraborty, M. (2020). Influence of graphene content on the mechanical properties of severely deformed graphene/aluminum composite. *Materials Chemistry and Physics*, *248*, 122939. https://doi.org/10.1016/j.matchemphys.2020.122939

[12] Tiwari, J. K., Mandal, A., & Chakraborty, M. (2019). Evaluation of mechanical and thermal properties of bilayer graphene reinforced aluminum matrix composite produced by hot accumulative roll bonding. *Journal of Alloys and Compounds*, *801*, 49-59. https://doi.org/10.1016/j.jallcom.2019.06.128

[13] Tiwari, J. K., Mandal, A., Sathish, N., & Chakraborty, M. (2018). Graphene platelets reinforced aluminum matrix composite with enhanced strength by hot accumulative roll bonding. *arXiv preprint*, *arXiv:1807*.00198. https://doi.org/10.48550/arXiv.1807.00198

[14] Ghaderi, O., Zare, M., Niroumand, B., Church, B. C., & Rohatgi, P. K. (2024). Selected challenges in solidification processing of graphene nanoplatelets (GNPs) reinforced aluminum alloys composites. *Frontiers in Materials*, *11*, 1363270. https://doi.org/10.3389/fmats.2024.1363270

[15] Singh, V. P., Gupta, G. K., & Mishra, S. (2025). Microstructural evolution and mechanical properties of multi-layered aluminum alloy 6061 processed by accumulative roll bonding. *Journal of Materials Engineering and Performance*, *34*(8), 6828-6839. https://doi.org/10.1007/s11665-024-09876-5

[16] Marcano, D. C., Kosynkin, D. V., Berlin, J. M., Sinitskii, A., Sun, Z., Slesarev, A., Alemany, L. B., Lu, W., & Tour, J. M. (2010). Improved synthesis of graphene oxide. *ACS Nano*, *4*(8), 4806-4814. https://doi.org/10.1021/nn1006368

[17] Donnet, J. B. (2018). *Carbon black: Science and technology* (2nd ed.). Routledge.

[18] Raei, M., Toroghinejad, M. R., & Jamaati, R. (2011). Nano/ultrafine structured AA1100 by ARB process. *Materials and Manufacturing Processes*, *26*(11), 1352-1356. https://doi.org/10.1080/10426914.2010.544820

[19] Eizadjou, M., Danesh Manesh, H., & Janghorban, K. (2009). Microstructure and mechanical properties of ultra-fine grains (UFGs) aluminum strips produced by ARB process. *Journal of Alloys and Compounds*, *474*(1-2), 406-415. https://doi.org/10.1016/j.jallcom.2008.06.147

[20] Uppada, S., Sivakumar, K., & Rajesh, K. (2025). Effect of accumulative roll bonding on microstructure and mechanical behavior of Al6061. *Journal of The Institution of Engineers (India): Series D*, *106*(1), 599-610. https://doi.org/10.1007/s40033-024-00789-4

[21] Scharnweber, J., Zlateva, G., & Göken, M. (2010). Texture, microstructure and mechanical properties of ultrafine grained aluminum produced by accumulative roll bonding. *Advanced Engineering Materials*, *12*(10), 989-994. https://doi.org/10.1002/adem.201000067

[22] Höppel, H. W., Hausöl, T., & Göken, M. (2020). The role of interfaces on the deformation mechanisms in bimodal Al laminates produced by accumulative roll bonding. *Advanced Engineering Materials*, *22*(9), 2000145. https://doi.org/10.1002/adem.202000145

[23] Ranjan, R., & Bajpai, V. (2021). Graphene-based metal matrix nanocomposites: Recent development and challenges. *Journal of Composite Materials*, *55*(17), 2369-2413. https://doi.org/10.1177/00219983211012345

[24] Wang, Z., Li, J., & Zhang, Y. (2024). Building a layer-structured aluminum/graphene composite with significant improvement in electrical conductivity. *Materials*, *17*(12), 2979. https://doi.org/10.3390/ma17122979

[25] Singh, V. P., Gupta, G. K., Mishra, S., & Kumar, A. (2026). Evolution of microstructure and mechanical properties of graphene oxide-reinforced aluminum alloy (6061) composite fabricated via accumulative roll bonding. *International Journal of Minerals, Metallurgy and Materials*, *33*(3), 935-952. https://doi.org/10.1007/s12613-025-3194-7

[26] Yang, Z., Liu, H., Chen, X., & Wang, L. (2025). Towards high performance nano multilayered graphene/5052 Al composite: In situ interfacial tailoring via accumulative roll bonding. *Carbon*, *238,* 120213. https://doi.org/10.1016/j.carbon.2025.120213